Multi-rank nuclear magnetic resonance studies of half-integer quadrupolar nuclei in solids by three-dimensional dynamic-angle correlation spectroscopy

Ales Medek, Joseph R. Sachleben, Peter Beverwyk, and Lucio Frydman[a)]
Department of Chemistry (M/C 111), University of Illinois at Chicago, 845 West Taylor Street, Chicago, Illinois 60607-7061

(Received 4 December 1995; accepted 4 January 1996)

The present work introduces a new three-dimensional nuclear magnetic resonance (3D NMR) experiment for the analysis of half-integer quadrupolar nuclei in solids. The method is based on the multi-rank expansion of the high-field NMR Hamiltonian governing the central transition of these spins in terms of irreducible spherical tensor elements. This approach leads to a temporal spin evolution given by an isotropic term characteristic of each chemical site, as well as by second- and fourth-rank anisotropies depending on the principal values and relative orientations of the shielding and quadrupolar interactions. A method for extracting the 3D spectral distribution correlating these three frequency components is presented, based on the acquisition of dynamic-angle spinning NMR signals collected as a function of different initial and final spinning axes. Computational and instrumental details involved in the acquisition of these 3D dynamic-angle correlation spectroscopy (DACSY) data are discussed, and applications of the DACSY methodology to the analysis of different rubidium salts are illustrated. The new type of chemical information that this experiment can provide and its relation to other NMR techniques that have been recently developed for the analysis of quadrupolar nuclei in solids are also discussed. [S0021-9606(96)01114-1]

I. INTRODUCTION

Magnetically active nuclides possessing spin numbers larger than 1/2 play a fundamental role in the analysis of a wide variety of technologically important materials. For a large number of solid systems including minerals, structural ceramics, semiconductors, glasses and catalysts, the nuclear magnetic resonance (NMR) spectroscopy of their constituent elements (^{11}B, ^{17}O, ^{23}Na, ^{27}Al, ^{87}Rb) has become the method of choice to characterize their chemical composition.[1,2] These NMR observations are usually complicated by the fact that such nuclei are quadrupolar, and therefore interact not only with locally induced magnetic fields but also with surrounding electric field gradients.[3] Although the size of these anisotropic quadrupolar couplings can prevent the extraction of chemically useful information from powder NMR spectra, most cases of interest are aided by the half-integer nature of the spins involved. In these cases it becomes possible to avoid the full effect of the quadrupolar couplings by restricting NMR observations to the central $-1/2 \leftrightarrow +1/2$ transition of the spin manifold, which is free to first order from quadrupole effects.[3–5]

Even these central transition experiments, however, will usually be broadened by anisotropic effects arising from chemical shift and second-order quadrupolar interactions. Numerous efforts have consequently been invested towards enhancing the chemical information that can be extracted from these central transition quadrupolar line shapes. A significant breakthrough in this field resulted from expanding the second-order quadrupolar Hamiltonian in terms of irreducible spherical tensors, an approach which enabled the recent development of a number of new high-resolution solid-state quadrupolar NMR methods.[6–10] The multi-rank expansion of the central transition quadrupolar Hamiltonian also helped to define the problem of second-order NMR effects within the same theoretical framework as the one used for treating more familiar first-order cases, like the chemical shift. Indeed, upon comparing the effects that first- and second-order NMR interactions can have on the spin evolution, the expansion in terms of irreducible tensors revealed that whereas the former generate frequency components involving an isotropic shift and a second-rank anisotropy, the latter introduce an additional term transforming as a fourth-rank tensor. Notably, although a large number of bidimensional methods for correlating the isotropic and anisotropic components of first-order Hamiltonians have been proposed, exemplified and employed in structural and dynamic chemical analyses,[11–16] no attention has been paid to similar multi-rank characterizations of the frequency terms arising from second-order Hamiltonians. The present article describes the first report of such multi-dimensional multi-rank NMR correlation, as applied to the central transition of half-integer quadrupolar nuclei.

We begin this presentation by reviewing the interactions governing quadrupolar NMR experiments, and by showing how expanding the central transition Hamiltonian in terms of its spherical tensor components leads to a picture whereby the evolution of the spins can be understood as a process taking place within a three-dimensional space that is Fourier paired to the various ranks of the spin Hamiltonian. Methods

[a)]To whom correspondence should be addressed.

 0021-9606/96/104(14)/5374/10/$10.00

for exploring this 3D time-domain are discussed, and a non-Cartesian approach capable of sampling a dense region of it using a series of bidimensional dynamic-angle spinning acquisitions is presented. An appropriate protocol for processing data acquired in this type of 3D dynamic angle correlation spectroscopy (DACSY) experiments is then introduced, and employed to obtain full 3D NMR correlation spectra between the different frequency ranks constituting the central transition nuclear spin Hamiltonian. The experimental implementation of this new NMR method is illustrated on a series of inorganic rubidium samples; the importance and potential applications of this experiment as well as its relation to other recent developments in the field are also discussed.

II. MULTI-RANK CORRELATIONS ON HALF-INTEGER QUADRUPOLAR SPINS

A. The three dimensions of central transition NMR experiments

The system that will be here considered consists of an ensemble of half-integer quadrupolar spins, placed inside a strong external magnetic field and subject to the effects of a quadrupolar and a shielding coupling. The total Hamiltonian $\mathscr{H}$ that then defines the NMR experiment can be summarized as

$$\mathscr{H}=\mathscr{H}_z+\mathscr{H}_q+\mathscr{H}_{\mathrm{cs}}, \tag{1}$$

where

$$\mathscr{H}_z=-\omega_0 S_z \tag{2}$$

is the dominant Zeeman coupling between the spins and the external field B_0, and $\mathscr{H}_q$, $\mathscr{H}_{\mathrm{cs}}$ represent the smaller quadrupolar and chemical shift interactions. Upon transforming this Hamiltonian into the usual Zeeman rotating frame, shielding and quadrupolar interactions will be truncated to their first-order secular expressions[17]

$$\begin{aligned}\mathscr{H}_{\mathrm{cs}}&=\gamma_S(R^{\mathrm{cs}}_{0,0}\cdot T^{\mathrm{cs}}_{0,0}+R^{\mathrm{cs}}_{2,0}\cdot T^{\mathrm{cs}}_{2,0})\\&=\Bigg[\omega^{\mathrm{iso}}_{\mathrm{cs}}+\frac{\Delta\omega_{\mathrm{cs}}}{2}(3\cos^2\beta_{\mathrm{cs}}-1\\&\quad+\eta_{\mathrm{cs}}\sin^2\beta_{\mathrm{cs}}\cos 2\alpha_{\mathrm{cs}})\Bigg]S_z\end{aligned} \tag{3}$$

and

$$\begin{aligned}\mathscr{H}_q&=\omega_q(R^q_{2,0}\cdot T^q_{2,0})\\&=\frac{\omega_q}{2}(3\cos^2\beta_q-1+\eta_q\sin^2\beta_q\cos 2\alpha_q)\\&\quad\times[3S_z^2-S(S+1)].\end{aligned} \tag{4}$$

In these equations $\omega^{\mathrm{iso}}_{\mathrm{cs}}$,$\Delta\omega_{\mathrm{cs}}$ are frequency parameters describing the isotropic and anisotropic chemical shifts, $\omega_q=(e^2qQ/h)/[2S(2S-1)]$ is the quadrupolar coupling constant, $(\eta_\lambda)_{\lambda=\mathrm{cs},q}$ are the asymmetry parameters of the shielding and quadrupolar interactions, and $(\alpha_\lambda,\beta_\lambda)_{\lambda=\mathrm{cs},q}$ are Euler angles relating the external magnetic field to the principal axis systems of the respective tensors.

Since quadrupole coupling constants in the MHz regime are fairly common, the interaction given by $\mathscr{H}_q$ will usually broaden single-quantum transitions between states with different values of S_z^2 ($\pm1/2\leftrightarrow\pm3/2$, $\pm3/2\leftrightarrow\pm5/2$, etc.) beyond the limits of detection. Central $-1/2\leftrightarrow+1/2$ transitions on the other hand will remain unaffected to first order by $\mathscr{H}_q$, thus endowing their spectroscopy with a much higher resolution and making their NMR observation a simple and widely used analytical approach in chemical investigations. Even the line shapes of these central transitions, however, are affected by quadrupole effects, which come into consideration via second-order perturbative terms proportional to ω_q^2/ω_0. The energy changes introduced by these second-order effects can be calculated from standard perturbation theory using the full expression of $\mathscr{H}_q$; this leads to a second-order Hamiltonian interaction of the form[18,19]

$$\begin{aligned}\mathscr{H}^{(2)}_q=\frac{\omega_q^2}{\omega_0}\{&R^q_{2,-1}R^q_{2,1}[T^q_{2,-1},T^q_{2,1}]\\&+R^q_{2,-2}R^q_{2,2}[T^q_{2,-2},T^q_{2,2}]/2\}.\end{aligned} \tag{5}$$

The products between spherical tensor elements $\{R^q_{l,m},T^q_{l,m}\}$ that appear in this expression can be further decomposed into their irreducible representations with the aid of appropriate Clebsch–Gordan coefficients. When this expansion is carried out on the spatial second-rank operator products $R^q_{2,-m}R^q_{2,m}$, the symmetry properties of angular momentum will only allow tensor elements possessing even-ranked values $l\leqslant4$ and null overall z components to be generated. The commutators containing the spin operators on the other hand will give rise to irreducible spherical components with ranks 1 and 3; for the $-1/2\leftrightarrow+1/2$ transition these operators are both proportional to S_z and thus lead to an overall central transition Hamiltonian $\mathscr{H}_{\mathrm{CT}}$ given by

$$\mathscr{H}_{\mathrm{CT}}=[(c^{\mathrm{cs}}_0R^{\mathrm{cs}}_{0,0}+c^q_0R^q_{0,0})+(c^{\mathrm{cs}}_2R^{\mathrm{cs}}_{2,0}+c^q_2R^q_{2,0})+c^q_4R^q_{4,0}]S_z, \tag{6}$$

where we have combined into a single expression the effects of $\mathscr{H}_{\mathrm{cs}}$ [Eq. (3)] and $\mathscr{H}^{(2)}_q$ [Eq. (5)], and introduced the $\{c^\lambda_i\}^{\lambda=\mathrm{cs},q}_{i=0-4}$ coefficients to take into account the appropriate proportionality constants. The Hamiltonian governing central transition quadrupolar NMR experiments is thus the sum of an isotropic term ($R^\lambda_{0,0}$) combining quadrupolar and shielding contributions, second-rank elements ($R^\lambda_{2,0}$) arising from chemical shift and quadrupolar anisotropies, and a fourth-rank term ($R^q_{4,0}$) originating solely from quadrupolar couplings.

The independent characterization of these different elements can reveal a wealth of information about the number of chemically inequivalent sites present in a sample and about their local electronic structure. Even a richer information can be expected if the various spectral ranks are not only independently measured but also correlated with each other by means of multidimensional spectroscopy, as this procedure could provide in a simple format all the chemical shift and quadrupolar information that can be retrieved by NMR from a powdered sample under fixed magnetic field operation. In accordance with this premise, we set out to develop

a 3D NMR protocol for obtaining these multi-ranked spectral correlations from quadrupolar nuclei. The proportionality of $\mathscr{H}_{\mathrm{CT}}$ with respect to the S_z operator suggests the inability of spin-space manipulations for distinguishing among the various spherical ranks. By contrast, the different behavior that characterizes each of the $\{R^{\lambda}_{i,0}\}_{i=0-4}$ terms with respect to spatial reorientations makes sample spinning a natural approach for their spectral differentiation. This assumption can be readily verified with the aid of the Wigner rotation matrices $\{\mathscr{D}^{i}_{m,m'}\}_{i=0-4}$.[20] For the sake of simplicity it is convenient to assume that the rate of macroscopic sample spinning ω_r fulfills the rapid-rotation condition $\omega_r \gg (\omega_q^2/\omega_0, \Delta\omega_{\mathrm{cs}})$; only terms proportional to $\{\mathscr{D}^{i}_{0,0}\}_{i=0-4}$ will then survive in the final expression of the average Hamiltonian, leading to a temporal evolution of the spins which can be described by a classical rotating-frame phase

$$\phi(t) = \omega^{(0)} \cdot t^{(0)} + \omega^{(2)}(\alpha,\beta) \cdot t^{(2)} + \omega^{(4)}(\alpha,\beta) \cdot t^{(4)}, \quad (7)$$

where following the notation employed in Eq. (6) we have grouped frequencies according to their rank, and introduced the three time-domain components

$$t^{(0)} = \int_0^t dt' = t, \quad (8)$$

$$t^{(2)} = \int_0^t P_2(\cos\,\theta)\, dt', \quad (9)$$

$$t^{(4)} = \int_0^t P_4(\cos\,\theta)\, dt'. \quad (10)$$

These three variables, which depend on the time t elapsed since spins are excited and on the spinning angle θ via second- and fourth-order Legèndre polynomials

$$P_2(\cos\,\theta) = (3\cos^2\,\theta - 1)/2, \quad (11)$$

$$P_4(\cos\,\theta) = (35\cos^4\,\theta - 30\cos^2\,\theta + 3)/8, \quad (12)$$

can be regarded as defining a three-dimensional **t** space where the temporal evolution of central transition NMR experiments takes place. The signal S that can be measured in this space from a quadrupolar spin ensemble is then the sum over all existing frequencies of a series of oscillating coherences

$$S(\mathbf{t}) = \int\int I(\omega^{(0)},\omega^{(2)},\omega^{(4)}) \exp\{i[\omega^{(0)} \cdot t^{(0)} + \omega^{(2)} \cdot t^{(2)} + \omega^{(4)} \cdot t^{(4)}]\} d\omega^{(0)}\, d\omega^{(2)}\, d\omega^{(4)}, \quad (13)$$

where the weighting coefficient $I(\omega^{(0)},\omega^{(2)},\omega^{(4)})$ represents the multi-rank correlation distribution between the various frequency components contributing to $\mathscr{H}_{\mathrm{CT}}$, and constitutes in consequence the 3D NMR spectrum that we are trying here to obtain.

An investigation of the different $(t^{(0)},t^{(2)},t^{(4)})$ elements reveals that the **t** space where the evolution of half-integer quadrupolar nuclei takes place cannot be densely sampled by changing the axis of sample rotation. Indeed variable-angle spinning (VAS) procedures only provide two independent parameters (the acquisition time t and the spinning axis θ) to drive the spin coherences throughout the 3D **t** space, thereby circumscribing the region that can be sampled in this manner to the parabolic surface illustrated in Fig. 1(A). This surface highlights the second limitation met by single-axis spinning strategies when applied on quadrupoles: since the region that can be sampled by VAS does not contain the $t^{(0)}$ axis, isotropic NMR spectra cannot be retrieved by monitoring central quadrupole transitions regardless of which spinning axis is chosen. This limitation was recently addressed by Pines, Virlet, and their co-workers,[6–8] who introduced two experiments capable of sampling the isotropic time evolution from quadrupolar spin ensembles by means of spatial manipulations. In one of their experiments, dynamic-angle spinning (DAS), the sample is spun during consecutive time intervals t_1 and t_2 about two different spinning axes, chosen to deprive the total spin evolution of anisotropic quadrupolar or shielding components. The second experiment, double rotation (DOR), achieves a similar refocusing of the anisotropic interactions by rapidly spinning a sample inside an inner rotor oriented at an angle θ_1 with respect to an outer rotor, that is itself spun at an angle θ_2 with respect to the magnetic field B_0. The averaging effects that both strategies have on the anisotropic evolution can be readily understood by consider-

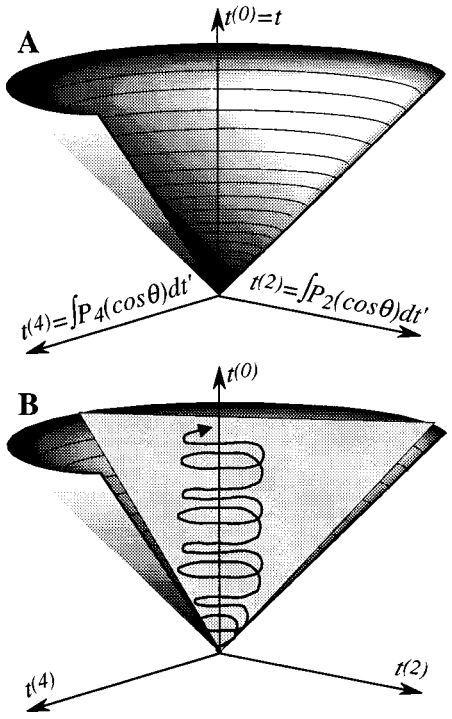

FIG. 1. (A) Three-dimensional $(t^{(0)},t^{(2)},t^{(4)})$ **t** space defining the evolution of central transition NMR experiments; the parabolic surface illustrates the region of this space that can be sampled by changing the spinning axis of a fast rotating sample. (B) Strategies available for sampling a dense region of the $(t^{(0)},t^{(2)},t^{(4)})$ time domain using spatial manipulations. The cross section indicated in gray depicts one of the surfaces that can be sampled by suddenly changing the axis of sample spinning (DAS); the continuous curve represents the time-domain trajectory generated by periodic variations of the spinning axis (DOR).

ing the three-dimensional **t**-space trajectories that they impart on the spins following their excitation [Fig. 1(B)]. DAS for instance constraints the spin evolution to take place within a plane that includes the $t^{(0)}$ axis, thus allowing one to digitize an isotropic signal in a point-by-point fashion; DOR accomplishes a similar sampling of the $t^{(0)}$ axis by carefully setting the inner and outer angles of rotation so as to impart on the spins a complex evolution that periodically crosses the isotropic time axis.

A common denominator between these two experiments is their introduction of a new degree of freedom, which allows one to ''steer'' the evolution of the spins throughout the 3D time domain. Both strategies can therefore be used not only to sample an isotropic unidimensional signal, but also to explore regions of the **t** space that lie within the interior of the parabolic surface accessible by VAS. This of course is one of the main conditions that must be met in order to fulfill our goal of retrieving $I(\omega^{(0)},\omega^{(2)},\omega^{(4)})$ NMR correlation spectra by Fourier analysis of 3D $S(\mathbf{t})$ time-domain signals. Due to its simpler experimental implementation, we decided to adopt the DAS-derived strategy in order to carry out the data acquisitions that are required by these 3D time-domain samplings. A graphic representation of the approach that resulted from this choice is depicted in Fig. 2(A). The pulse sequence itself is analogous to the one involved in 2D DAS; it consists of an initial evolution period during which the sample is spun at an angle θ_1, a storage period where the spinning axis is reoriented, and a signal detection period with the sample spinning at a second angle θ_2. By applying the standard rules of radio-frequency (rf) phase cycling it is possible to select only those density matrix elements that undergo an anti-echo coherence transfer pathway $-1(t_1)\rightarrow 0(\text{storage})\rightarrow -1(t_2)$;[21] for these elements a proper choice of initial and final spinning angles fulfilling

$$P_2(\cos\,\theta_1)t_1+P_2(\cos\,\theta_2)t_2=0, \tag{14}$$

$$P_4(\cos\,\theta_1)t_1+P_4(\cos\,\theta_2)t_2=0, \tag{15}$$

can refocus the second- and fourth-rank anisotropies while preserving a net isotropic evolution. The fact that Eqs. (14) and (15) possess more variables than constraints implies that complementary pairs $\{\theta_1,\theta_2\}$ of DAS spinning angles are not unique, but can be chosen from within a range $\{0°\leqslant\theta_1\leqslant 39°,\ 63°\leqslant\theta_2\leqslant 90°\}$.[8,18] Within our picture of central transition quadrupolar NMR experiments as taking place within a 3D **t** space, this freedom of choice reflects the possibility of sampling an isotropic signal using different bidimensional cross sections rotated with respect to one another by different amounts with respect to the $t^{(0)}$ axis [Fig. 2(B)]. This in turn implies that a dense volume of the 3D **t** space can be sampled by using a series of bidimensional DAS NMR signals; this is the procedure that we adopted as the basis of dynamic-angle correlation spectroscopy (DACSY), the new method that we developed for obtaining 3D multi-rank correlation spectra between the constituents of $\mathscr{H}_{\mathrm{CT}}$.

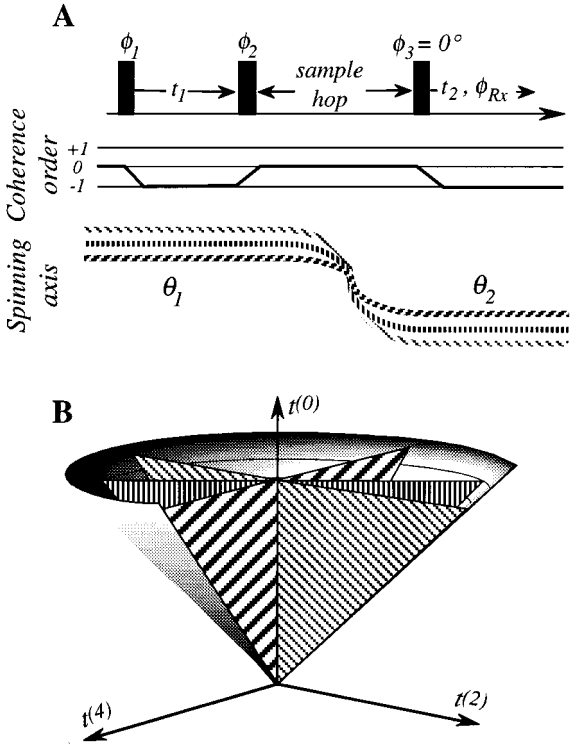

FIG. 2. (A) Experimental basis for the acquisition of 3D DACSY NMR spectra on quadrupolar spins. The pulse sequence (top) is analogous to the one used in 2D DAS NMR; it contains three 90° radio frequency pulses with relative phases cycled so as to select anti-echo coherence transfer pathways, and initial and final sample spinning angles chosen so as to average out second- and fourth-rank anisotropies. (B) Sequence of **t**-space cross sections that can be sampled by carrying out a series of 2D DAS acquisitions employing different pairs of complementary (θ_1,θ_2) spinning angles.

B. Acquisition and processing of 3D DACSY NMR data

In order to obtain the desired $I(\omega^{(0)},\omega^{(2)},\omega^{(4)})$ distribution from DAS data collected as a function of θ_1, θ_2, t_1, and t_2, it is necessary to Fourier transform the experimental points with respect to the three components $(t^{(0)},t^{(2)},t^{(4)})$ that make up the relevant 3D time-domain space. Although a straightforward way of carrying out such an analysis is by using the fast Fourier transform (FFT) algorithm, the non-Cartesian manner in which DAS experiments sample the 3D time-domain does not position the digitized points along the equally spaced grid that is required by this computational procedure. This limitation can be solved by sampling in a sufficiently dense manner a region of the time domain that is large enough to support the desired spectral resolution, and by subsequently interpolating the digitized points into a regular grid suitable for FFT. As in the case of conventional 3D NMR spectroscopy, the spacing and total number of data that are transformed in the 3D time-domain will end up determining the characteristics of the frequency-domain distributions. Consequently, we define the grid to be interpolated in terms of a dwell time vector $(\Delta t^{(0)},\Delta t^{(2)},\Delta t^{(4)})$ chosen to suit the width of the various features in the final NMR spectrum, and in terms of a size $N^{(0)}\times N^{(2)}\times N^{(4)}$ that will define the final resolution along the different spectral axes. The lin-

ear dependence of $t^{(0)}$ on the physical evolution and detection times t_1 and t_2 ensures that all experimental data can be distributed along equally spaced planes of points, provided that the condition

$$\Delta t_1 = \Delta t_2 = \Delta t^{(0)} \tag{16}$$

is chosen upon setting up the experimental DAS acquisitions [Fig. 3(A)]. Interpolation of the experimentally digitized points into a regular grid is thus reduced from a three-dimensional problem to a two-dimensional one, no manipulations being necessary along the $t^{(0)}$ axis. The pattern that experimental points will then create on the $(t^{(2)},t^{(4)})$ planes is illustrated in Fig. 3(B). Only the shaded area becomes accessible by the DACSY protocol, a limitation which stems from our choice of restricting DACSY acquisitions to pairs of complementary DAS angles fulfilling Eqs. (14) and (15), and to elements of the density matrix corresponding to anti-echo coherence transfer pathways. Rather than trying to extend this domain of sampled data to other regions of the **t** space we chose to set the grid points falling outside the digitized areas to zero before the FFT; numerical simulations revealed that very small artifacts result from this approximation.

In order to estimate the NMR signal on each of the grid points to be Fourier transformed, a search procedure for identifying the four experimental points that are closest to the coordinate of interest was implemented. The signal evaluation procedure was then carried out using three simple linear interpolations [Fig. 3(C)]: the first two provided the values that the NMR signal would have measured along neighboring DAS data sets at a distance from the origin equal to the one corresponding to the grid point of interest, while the last one weighted these two numbers according to their angular dispersion with respect to the grid's coordinate. These numerical computations solved the only unusual complication thus involved in 3D DACSY NMR experiments, which result from the radial manner in which data are sampled along the $(t^{(2)},t^{(4)})$ planes. This kind of sampling is strongly reminiscent to the one occurring in 2D variable-angle correlation spectroscopy and in back-projection NMR imaging;[15,22] in analogy with the procedures employed in these methodologies, we decided to select the N experimental pairs of spinning angles $\{\theta_1,\theta_2\}$ that are involved in a 3D DACSY acquisition so as to sample the time domain in the most uniform possible way. The slopes that the different DAS acquisitions constituting the total 3D experiment subtend in a $(t^{(2)},t^{(4)})$ plane are therefore required to fulfill the relation

$$\text{slope}_i = \text{slope}_{\min} + (\text{slope}_{\max} - \text{slope}_{\min}) \cdot (i-1)/(N-1),$$

$$i = 1,2,\ldots,N, \tag{17}$$

where $\text{slope}_{\max}$, $\text{slope}_{\min}$ define the limits of the $(t^{(2)},t^{(4)})$ region to be sampled, and are given by the smallest and largest value used for θ_1 and by the value chosen for the $\Delta t^{(2)}/\Delta t^{(4)}$ ratio. This condition, coupled to Eqs. (14) and (15), unequivocally determines all the spinning angles that must be used throughout the multidimensional NMR acquisition.

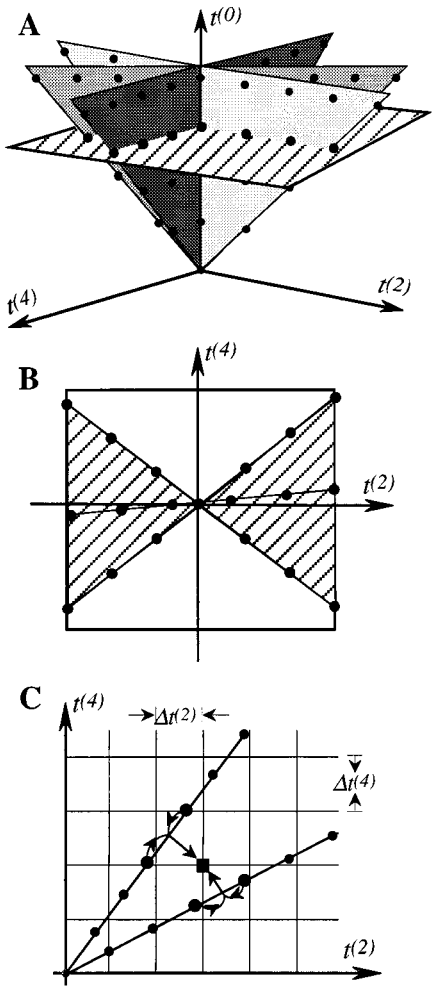

FIG. 3. (A) Digitization of the time domain in 3D DACSY NMR. Equal increments in the t_1 and t_2 times of the various 2D DAS acquisitions ensure that 3D DACSY points are arranged in equidistant planes of data along the $t^{(0)}$ axis. (B) Distribution of points within a $(t^{(2)},t^{(4)})$ plane. The choice of restricting acquisitions to complementary pairs of DAS angles circumscribes the sampling to the shaded area; the interior of this region is monitored in the most uniform possible way, while points outside this region are arbitrarily set to zero. (C) Mapping of the experimental DACSY data into a Cartesian grid of $S(t^{(2)},t^{(4)})$ points. The value of the signal at a particular grid coordinate (square) is estimated from the four nearest experimental points (large dots) by performing three successive linear interpolations (arrows).

III. EXPERIMENT

To test the feasibility and potential applications of the methodology introduced in the preceding section, 3D ^{87}Rb DACSY NMR spectra were collected on a series of different rubidium salts (^{87}Rb: $S=3/2$ isotope, $\approx$30% natural abundance). 7.1 and 4.7 T NMR spectrometers were employed in these determinations. The laboratory-built rf components of these instruments were controlled by Tecmag Inc. pulse programmers; this NMR hardware was also connected to

Whedco Inc. motor and motor controller systems that allowed us to hop samples between different spinning axes with a 0.2° accuracy within a 45 ms hopping (plus settling) time. Three-pulse DAS sequences were employed in all the experiments, with a sixteen scan irradiation and demodulation phase cycle chosen to select the $-1(t_1) \rightarrow 0(\text{mixing}) \rightarrow -1(t_2)$ coherence transfer pathway. The central transition 90° pulses that were used lasted between 1.7 and 4 μs, depending on the angle of sample spinning.

The laboratory-built NMR probeheads used in the present work employed a single irradiation/reception rf coil wound around a 5 or a 7 mm Doty zirconia stator; the latter was inserted inside a Kel-F housing and coupled by a string-driven pulley system to a stepping motor at the base of the probehead body. Samples were spun at rates of either 5 or 10 kHz, depending on the type of stator system used. Typical DACSY acquisition parameters involved the collection of 31 independent DAS experiments with initial and final spinning angles spread over a $\{18° \leqslant \theta_1 \leqslant 39°,\ 65° \leqslant \theta_2 \leqslant 90°\}$ range; each of these DAS experiments involved 31 t_1 increments and 128 directly digitized t_2 points separated by 45 μs dwell times. When considering that a semi-dilute isotope like ^{87}Rb requires a few hundred scans to yield DAS NMR data with good signal-to-noise ratios and that each scan requires changing the macroscopic axis of rotation from θ_1 to θ_2 and back, it follows that a typical 3D DACSY NMR acquisition can involve approximately half a million uninterrupted hops of a spinning sample. The implementation of such a demanding procedure was initially attempted using conventional flexible leads for connecting the rf sample coil to the rest of the probehead electronics, but this approach failed due to repetitive lead breakage. The probeheads were therefore modified into an arrangement based on sliding contacts like the one schematized in Fig. 4(A), which undergoes negligible mechanical deformations upon changing the axis of sample spinning. We found that this design allowed the sample to undergo literally millions of uninterrupted jumps, while endowing the NMR probehead with a remarkable tuning independence [Fig. 4(B)] at the expense of almost no degradation to the overall electronic performance of the resonant circuit.

The total acquisition time required by the 3D NMR experiments that are illustrated below ranged between 2 and 5 days. After completing these acquisitions the collected data were transferred to a Silicon Graphics R3000 computer, where the interpolation procedure described above was carried out. The result of these calculations consisted of 128 $\times 63 \times 63$ arrays of complex data; these were zero filled into 128^3 cubes, weighted and Fourier transformed using graphic NMR modules running under the Silicon Graphic's Explorer program environment.

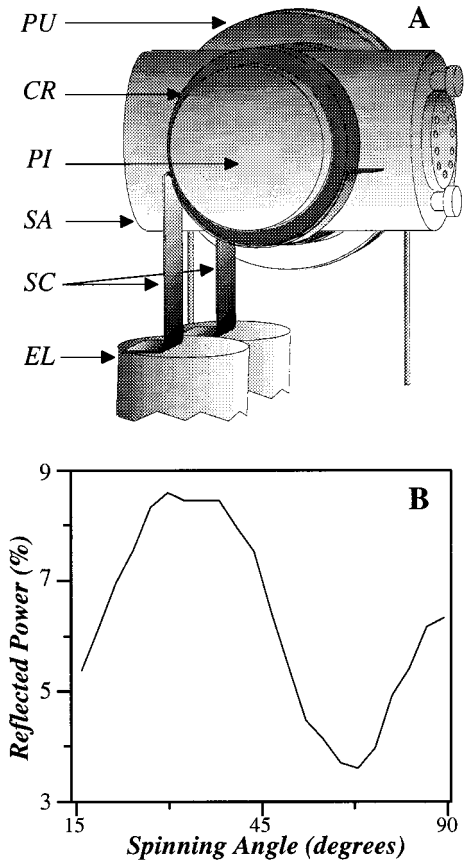

FIG. 4. (A) Sliding-contacts design adopted for the implementation of 3D DACSY NMR experiments. Abbreviations indicate the electronic components of the probehead circuit (EL), the sliding contacts (SC), the spinning assembly containing the stator (SA), the axle around which the sample pivots (PI), the copper rings interfacing the rf sample coil with the sliding contacts (CR), the pulley system connecting the spinning assembly to a stepping motor at the base of the probe (PU). (B) Percentage of incoming rf power that is reflected from the assembly shown in part (A), as a function of the angle θ between the spinner and the magnetic field. The system was initially tuned at $\theta = 90°$ by minimizing the rf power reflected at the ^{87}Rb Larmor frequency.

IV. RESULTS

Figure 5 illustrates the different stages that are involved in the acquisition of a 3D DACSY NMR spectrum, using the single-site system $RbClO_4$ as an example. The plot in part (A) illustrates an experimental set of data as collected in the spectrometer as a function of different $\{\theta_1, \theta_2, t_1, t_2\}$ values. Once these data became available they were used to estimate the signal $S(\mathbf{t})$ over a regular grid of 3D data points in the $(t^{(0)}, t^{(2)}, t^{(4)})$ space, using the procedure described above [Fig. 5(B)]. Notice that since the range of spinning angles employed in the 2D acquisitions correspond to both positive and negative values of $P_2(\cos\theta)$ and $P_4(\cos\theta)$, effective echoes are generated along the $t^{(2)}$ and $t^{(4)}$ time axes. This refocusing allows one to retrieve spectral line shapes that are largely devoid from dispersive components, without the additional need of acquiring complementary sets of 3D time-domain data. Once this interpolated array is obtained the data processing continues as in conventional multidimensional spectroscopy, with apodization, zero-filling and FFT affording the desired ^{87}Rb 3D NMR spectrum [Fig. 5(C)]. This spectrum shows a single sharp resonance along its isotropic frequency axis possessing a line width of about 300 Hz, a degree of resolution that is characteristic of conventional

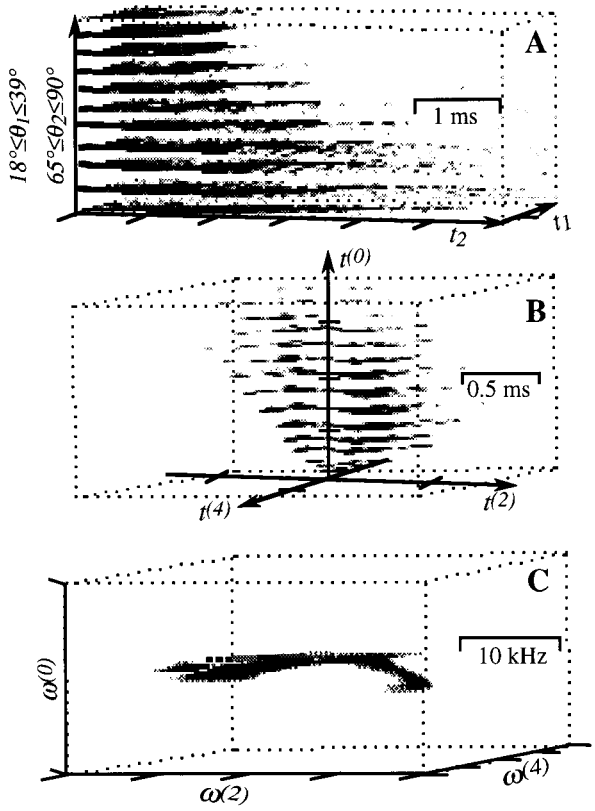

FIG. 5. Stages involved in the retrieval of a 3D multi-rank ^{87}Rb NMR correlation spectrum on $RbClO_4$ at 7.1 Tesla. (A) Experimental set of 2D time-domain DAS signals recorded as a function of different initial and final spinning angles $\{\theta_1,\theta_2\}$; notice how the slopes of the isotropic echoes, indicated by dark ridges in the (t_1,t_2) planes, change throughout the NMR acquisitions. (B) 3D time-domain DACSY set obtained after mapping the experimental data shown in part (A) onto the $(t^{(0)},t^{(2)},t^{(4)})$ space. (C) Gray scale isosurface of the 3D multi-rank correlation spectrum obtained by Fourier transformation of the data shown in part b.

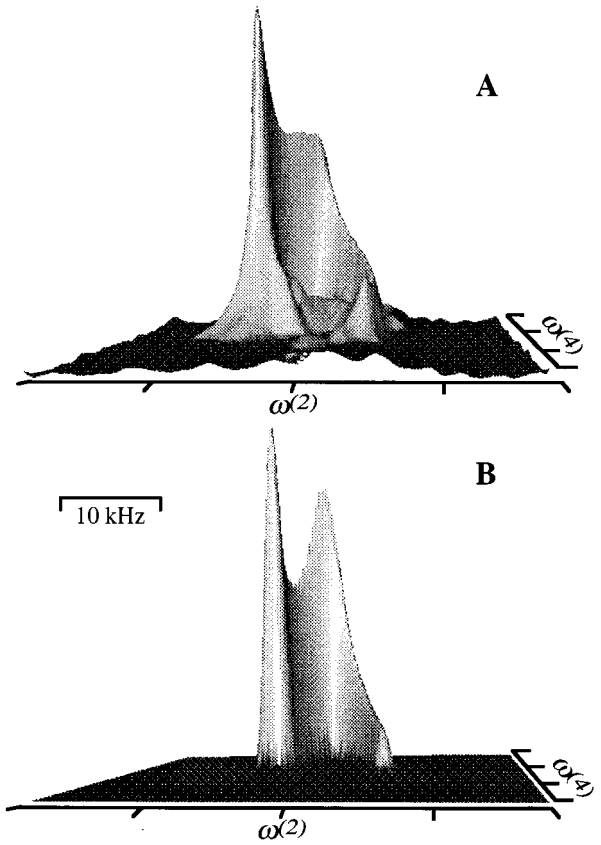

FIG. 6. (A) Experimental second-/fourth-rank correlation distribution extracted at the isotropic frequency of the $RbClO_4$ 3D DACSY resonance. (B) Idealized second-/fourth-rank NMR line shape calculated using the $RbClO_4$ parameters reported in Table I.

^{87}Rb DAS acquisitions. Perpendicular to this isotropic coordinate, the 3D NMR spectrum makes available a featured 2D powder pattern along the $(\omega^{(2)},\omega^{(4)})$ frequency plane [Fig. 6(A)]. The line shape arising from this bidimensional distribution is particularly interesting, as it correlates for all crystallites in the sample the fourth-rank line shape originating from the quadrupolar coupling with traditional Blombergen–Rowland second-rank line shapes stemming from the sum of the quadrupolar and chemical shift anisotropies. One can expect these novel powder patterns to be highly sensitive to the anisotropies and asymmetry parameters of both the chemical shift and quadrupolar tensors, as well as to the Euler angles (ξ,χ,ψ) defining their relative orientations. For the particular case of $RbClO_4$, the experimental $I(\omega^{(2)},\omega^{(4)})$ ^{87}Rb NMR line shape can be simulated using chemical shift anisotropy and quadrupolar parameters similar—though not identical—to those reported in the literature [Fig. 6(B)].[23–25] The excellent agreement that can be observed between the experimental $RbClO_4$ spectral slice and idealized $I(\omega^{(2)},\omega^{(4)})$ distributions arising from optimized literature values justify our data acquisition and processing approach; the only artifacts that can be ascribed to the incomplete sampling of the 3D **t** space take the form of small ridges departing diagonally from the main resonance powder peak.

Figures 7 and 8 show additional applications of this new form of 3D solid phase NMR spectroscopy, this time to the analysis of the multisite rubidium salts Rb_2SO_4 and $RbNO_3$. The spectral resolution that in both cases can be observed along the isotropic frequency axis is comparable to the one observed in conventional DAS NMR, while data planes extracted perpendicular to the isotropic coordinates of the different chemical sites display 2D line shapes encoding and correlating the anisotropic ranks arising from the quadrupolar and chemical shift tensors. The richness of these 2D powder correlations afforded by DACSY can be further appreciated in Fig. 9, which compares the anisotropic patterns that were resolved in these experiments for different rubidium sites with simulated distributions calculated to obtain optimized visual fits. In all these cases we found that simulations which take into account quadrupolar and shielding interactions of appropriate sizes can reproduce the ridges and splittings observed in the experimental powder patterns, provided that the relative orientations between the two tensors are carefully adjusted.

TABLE I. Quadrupolar and shielding parameters derived from anisotropic ^{87}Rb 3D DACSY line shape simulations.[a]

Compound	Site	$\Delta\omega_{cs}$[b] (ppm)	η_{cs}[b]	e^2qQ/h (MHz)	η_q	(ξ,χ,ψ)[c] (deg)
$RbClO_4$	···	−20±10	0.±0.1	3.5±0.1	0.2±0.1	(0±10,90±15,0±10)
Rb_2SO_4	Rb(1)	−40±10	0.5±0.1	2.7±0.1	0.9±0.1	(25±10,90±10,25±10)
$RbNO_3$	Rb(1)	28±7	0.6±0.1	1.8±0.1	0.3±0.1	(0±10,25±10,60±10)
	Rb(2)	31±7	0.5±0.1	1.9±0.1	0.5±0.1	(90±15,15±5,45±15)
	Rb(3)	46±3	0.4±0.1	2.4±0.1	0.7±0.1	(45±15,15±5,45±15)

[a]Error margins reflect the range of meaningful line shape fits.
[b]Assuming the conventions $\Delta\omega_{cs}=\omega_{33}-\omega_{cs}^{iso}$; $\eta_{cs}=|(\omega_{22}-\omega_{11})/\Delta\omega_{cs}|$; $|\omega_{33}-\omega_{cs}^{iso}|\geqslant|\omega_{22}-\omega_{cs}^{iso}|\geqslant|\omega_{11}-\omega_{cs}^{iso}|$.
[c]Euler angles relating the chemical shielding and quadrupolar tensors.

V. DISCUSSION AND CONCLUSIONS

The main objective of the present paper was to describe a new approach for characterizing chemically inequivalent quadrupolar sites in powdered samples by means of multidimensional NMR. In order to achieve this goal we revisited the way in which central transition NMR experiments on half-integer quadrupoles are described, using the multi-rank expansion of the relevant Hamiltonian in terms of irreducible tensor components as a starting point. This approach lead to a picture whereby the evolution of excited quadrupolar spins could be represented by vectors moving throughout a multidimensional time-domain space, a theoretical framework which when coupled to modern ideas regarding the non-Cartesian sampling of **t** spaces[26] allowed us to derive a new 3D solid-phase NMR technique for correlating the various frequency ranks contributing to the total spin Hamiltonian. The $I(\omega^{(0)},\omega^{(2)},\omega^{(4)})$ distributions that resulted from these considerations play for the NMR spectroscopy of half-integer quadrupoles a role that is completely analogous to the one played by well-known forms of isotropic–anisotropic chemical shift correlation spectroscopy on spin-1/2 nuclei. Just as in the case of the latter, the 3D NMR distributions made available by DACSY can reveal for inequivalent chemical sites a valuable information about their electronic

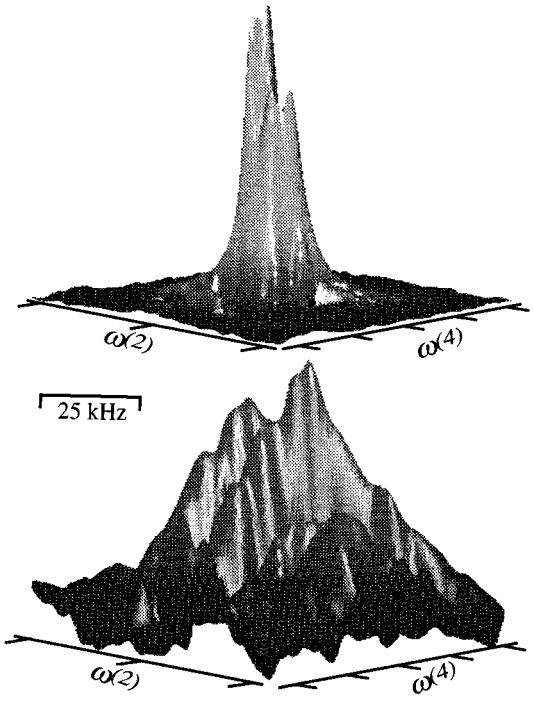

FIG. 7. Experimental second-/fourth-rank ^{87}Rb NMR powder line shapes resolved for the two inequivalent sites of Rb_2SO_4. Spectra were obtained at 7.1 Tesla by extracting slices at the appropriate isotropic frequencies of the 3D DACSY NMR spectrum.

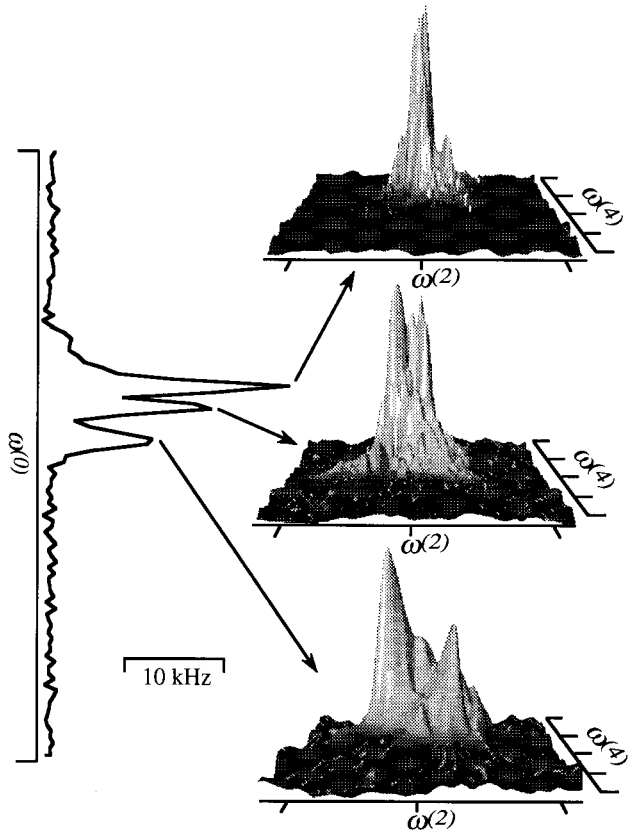

FIG. 8. Schematic representation of the 3D DACSY NMR results obtained on a $RbNO_3$ sample at 4.7 Tesla. The vertical trace corresponds to the projection of the 3D frequency data set onto the isotropic $\omega^{(0)}$ axis; the 2D anisotropic line shapes on the right correspond to the second-/fourth-rank correlation distributions extracted at the isotropic frequencies indicated by the arrows.

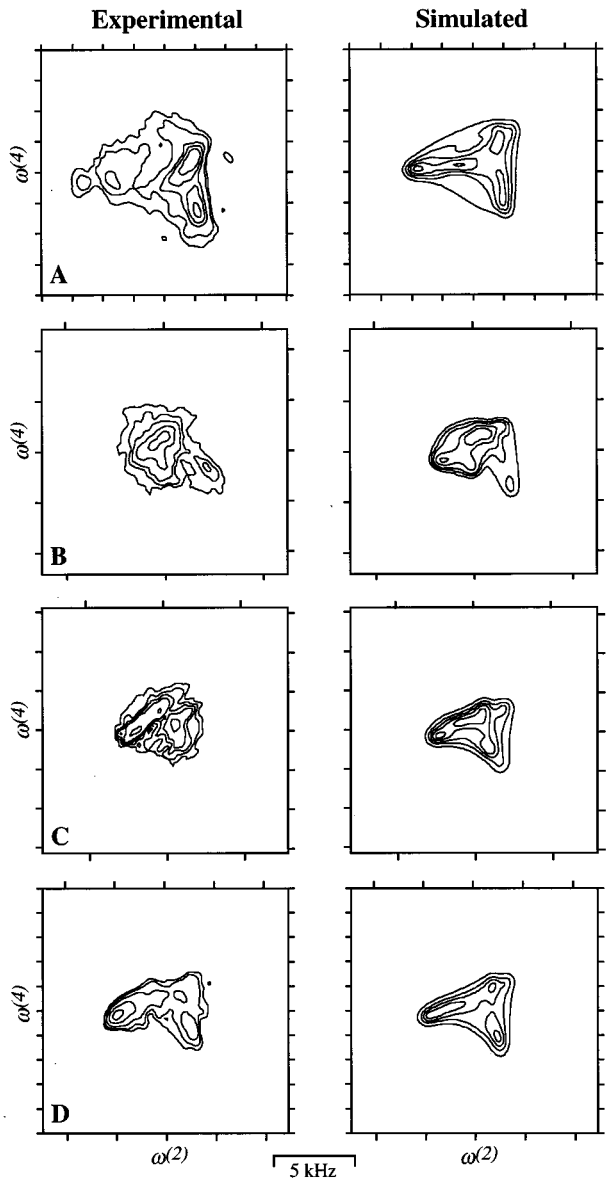

FIG. 9. Comparison between the experimental second-/fourth-rank correlations afforded by 3D DACSY NMR for (A) site 1 of Rb_2SO_4 (top trace, Fig. 7) and [(B)–(D)] the three sites of $RbNO_3$ (Fig. 8), and best-fit simulated distributions. Fits were selected on the basis of visual comparisons and employed the shielding and quadrupolar parameters listed in Table I.

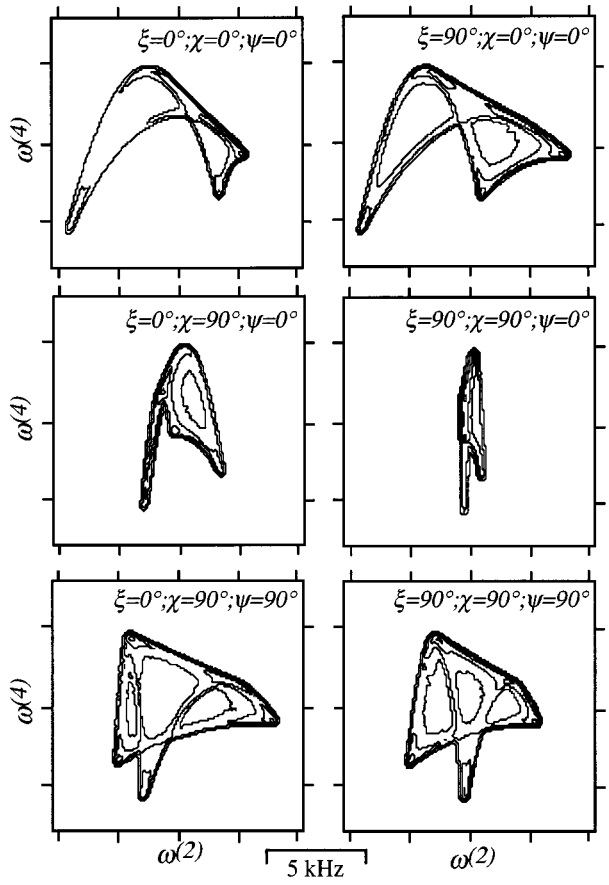

FIG. 10. Simulated set of second-/fourth-rank 2D correlation distributions calculated for typical shielding and quadrupolar ^{87}Rb coupling parameters ($\omega_0=98$ MHz, $\Delta\omega_{cs}=-50$ ppm, $e^2qQ/h=2.5$ MHz, $\eta_q=\eta_{cs}=0.5$), as a function of the indicated Euler angles between the two tensors.

environments with a degree of detail which is only comparable to that available from single-crystalline measurements. Also in analogy to what happens with 2D isotropic-anisotropic chemical shift correlation spectroscopy, we expect 3D DACSY NMR to become a valuable starting point for the characterization of internuclear geometries and of molecular dynamics in multi-site systems.

The ^{87}Rb DACSY NMR line shapes that were illustrated in the preceding section carry a highly accurate description of the quadrupolar and shielding parameters of each chemical site, as well as valuable information about the relative orientation between the principal axis systems of these two tensors. Figure 10 illustrates the high degree of sensitivity that the anisotropic frequency components of DACSY line shapes can be expected to display with respect to these angular parameters, using a set of distributions computed for identical chemical shift and quadrupolar couplings but assuming different relative tensor orientations. A similar sensitivity was recently observed by Pines and co-workers using 2D switched-angle-spinning NMR,[27] an approach that is closely related to both 2D DAS and to the 3D DACSY experiment here presented. Overall it is likely that the advent of these new forms of multidimensional analysis will complement each other, and open new opportunities regarding the use of quadrupolar NMR toward the chemical characterization of solid materials.

ACKNOWLEDGMENTS

The present research was supported by the National Science Foundation through Grant Nos. DMR-9420458 and CHE-9502644 (CAREER Award); L.F. is a Camille and Henry Dreyfus New Faculty Awardee (1992–1997).

[1] *Multinuclear Magnetic Resonance in Liquids and Solids—Chemical Applications*, edited by P. Granger and R. K. Harris (Kluwer Academic, Dodrecht, 1990).

[2] *NMR Techniques in Catalysis*, edited by A. T. Bell and A. Pines (Marcel Dekker, New York, 1994).
[3] A. Abragam, *The Principles of Nuclear Magnetism* (Oxford U.P., Oxford, 1985).
[4] G. E. Maciel, Science **226**, 282 (1984).
[5] E. Oldfield and R. J. Kirkpatrick, Science **227**, 1537 (1985).
[6] A. Llor and J. Virlet, Chem. Phys. Lett. **152**, 248 (1988).
[7] A. Samoson, E. Lippmaa, and A. Pines, Mol. Phys. **65**, 1013 (1988).
[8] K. T. Mueller, B. Q. Sun, G. C. Chingas, J. W. Zwanziger, T. Terao, and A. Pines, J. Magn. Reson. **86**, 470 (1990).
[9] B. F. Chmelka, K. T. Mueller, A. Pines, J. Stebbins, Y. Wu, and J. W. Zwanziger, Nature **339**, 42 (1989).
[10] L. Frydman and J. S. Harwood, J. Am. Chem. Soc. **117**, 5367 (1995).
[11] E. L. Lippmaa, M. Alla, and T. Tuhrem, *Proceedings of the 19th Congress Ampere* (Springer-Verlag, Heidelberg, 1976).
[12] Y. Yarim-Agaev, P. N. Tutunjian, and J. S. Waugh, J. Magn. Reson. **47**, 51 (1982).
[13] A. Bax, N. M. Szeverenyi, and G. E. Maciel, J. Magn. Reson. **52**, 147 (1983).
[14] R. Tycko, G. Dabbagh, and P. A. Mirau, J. Magn. Reson. **85**, 265 (1989).
[15] L. Frydman, G. C. Chingas, Y. K. Lee, P. J. Grandinetti, M. A. Eastman, G. A. Barrall, and A. Pines, J. Chem. Phys. **97**, 4800 (1992).
[16] Z. Gan, J. Am. Chem. Soc. **114**, 8307 (1992).
[17] M. Mehring, *High Resolution NMR in Solids* (Springer, Berlin, 1983).
[18] B. Sun, Ph.D. thesis, Lawrence Berkeley Laboratory, University of California (1991).
[19] M. Goldman, P. J. Grandinetti, A. Llor, Z. Oleniczak, J. R. Sachleben, and J. W. Zwanziger, J. Chem. Phys. **97**, 8947 (1992).
[20] U. Haeberlen, in *Advances in Magnetic Resonance*, edited by J. S. Waugh (Academic, New York, 1976).
[21] R. R. Ernst, G. Bodenhausen, and A. Wokaun, *Principles of Nuclear Magnetic Resonance in One and Two Dimensions* (Clarendon, Oxford, 1987).
[22] P. T. Callaghan, *Principles of Nuclear Magnetic Resonance Microscopy* (Oxford U.P., Oxford, 1991).
[23] J. H. Baltisberger, S. L. Gann, E. W. Wooten, T. H. Chang, K. T. Mueller, and A. Pines, J. Am. Chem. Soc. **114**, 7489 (1992).
[24] J. T. Cheng, J. C. Edwards, and P. D. Ellis, J. Phys. Chem. **94**, 553 (1990).
[25] T. Vosegaard, J. Skibsted, H. Bildsøe, and H. J. Jakobsen, J. Phys. Chem. **99**, 10731 (1995).
[26] L. Frydman and J. Peng, Chem. Phys. Lett. **220**, 371 (1994).
[27] J. S. Shore, S. Wang, R. E. Taylor, A. T. Bell, and A. Pines, J. Chem. Phys. (in press).